Comparison of Fuel Consumption of Continuous Descent Operations with Required Times of Arrival

Path Stretching vs. Powered Descents

Raúl Sáez and Xavier Prats
Department of Physics - Aerospace division
Technical University of Catalonia - BarcelonaTECH
Castelldefels, Spain 08860
raul.saez.garcia@upc.edu and xavier.prats@upc.edu

***Abstract*—Continuous descent operations (CDOs) with required times of arrival (RTAs) have proven to deliver major environmental benefits in terminal maneuvering areas (TMAs) without degrading capacity. When traffic density is high, air traffic controllers (ATC) have to delay flights and assign an RTA different from the aircraft's estimated time of arrival (ETA). In such case, aircraft may have to follow a non-optimum speed profile and possibly be forced to fly powered descents instead of neutral CDOs. Furthermore, ATC may also stretch the planned route to keep the safety of the operation. In that case, aircraft might be able to fly neutral CDOs, but at the expense of flying a longer route. In this paper, the differences in fuel consumption between powered descents and path stretching are quantified. A simplified scenario has been defined in which an Airbus A320 is approaching a generic airport with a finite number of arrival routes (i.e. distances to go), and several fictitious RTAs. Then, an optimal control problem has been formulated and solved in order to generate several trajectories meeting the assigned RTAs. In terms of fuel consumption results show that, for RTAs later than the ETA, although in the beginning path stretching represents a higher fuel consumption, in the end flying powered descents is the strategy that consumes more fuel. For RTAs earlier than the ETA, path stretching shows lower consumption values. The methodology presented in this paper could help to define a ground supporting tool to help ATC to decide which would be the best decision under the trajectory based operations paradigm.**

Keywords-Continuous descent operations; Required time of arrival; Path stretching; Fuel efficiency

I. Introduction

A continuously growing environmental sensitivity in aviation has encouraged the research into methods for achieving a greener air transportation. Continuous descent operations (CDOs) allow aircraft to follow an optimum flight path that delivers major environmental and economic benefits, giving as a result engine-idle descents that reduce fuel consumption, pollutant emissions and noise nuisance[1], [2], [3]. This need for a cleaner aviation is clearly recognized by the SESAR [4] and NextGen programs [5], which aim to reduce the environmental impact of aviation while increasing capacity and safety. A key transformation to achieve these goals is the use of new air traffic management (ATM) paradigms such as the trajectory based operations (TBO) concept.

CDOs are optimized to the operating capability of the aircraft, resulting in different optimum trajectories for aircraft with different characteristics. As a result, the vertical and time predictability of incoming traffic flows decreases, which leads to an increase of the air traffic controller officer (ATCO) workload. Consequently, ATCOs would increase separation buffers leading to airspace and runway capacity loses that are not acceptable in major terminal maneuvering areas (TMAs), especially during peak hours. A solution for this problem, aligned with the TBO paradigm, would be to sequence and merge arrival traffic by assigning required times of arrival (RTAs) at one or several fixes along a known route (2D trajectory), which would improve the predictability of the arriving aircraft. This allows the flight management system (FMS) to know the remaining distance to go, and thus, enable the aircraft to fly an optimal descent profile while satisfying the RTA [6].

Given a merging fix, if the RTA is close to the estimated time of arrival (ETA) at that fix for the planed (thrust idle) descent, the aircraft will be able to adapt the trajectory and still fly a neutral CDO (i.e. idle thrust and without using speed-brakes). In [7] it was reported that for certain conditions this RTA can be updated even when the descent has been initiated and still find solutions not requiring thrust or speed-brakes. However, for certain aircraft energy states (i.e. altitude/speed conditions) or for those RTAs significantly differing from the ETA, a neutral CDO is not possible. Furthermore, for certain traffic loads and TMA sizes it would not be possible either to sequence all arriving traffic using only RTAs leading to neutral CDOs, as reported for instance in [8].

This paper compares two possible solutions to accommodate arrivals when not all aircraft can fly neutral CDOs following the planned route: i) aircraft flying the planned route but with descents requiring thrust or speed-brake usage to fulfill the RTA (i.e. powered descents); and ii) stretching the arrival route to fly longer distances and fulfill the same RTA, but enabling neutral CDOs. The differences in fuel consumption are quantified for both cases. This work represents a first step to define a ground supporting tool to help ATC to decide which would be the best decision under the TBO paradigm,

where advanced synchronisation mechanisms between ground and airborne tools are expected.

To the best of the authors' knowledge, no other works analyzed the trade-offs between path stretching vs. the use of powered descents. A similar study was done in [9], where an assessment of the difference in fuel consumption between neutral CDOs and powered descents was presented, but it is not concluded when it would be more desirable to fly this kind of procedures instead of stretching the route for different RTA values. Another similar study was done in [10], where fuel consumption is quantified for descent trajectories with an assigned RTA later than the ETA at the metering fix. However, the paper does not focus on CDOs specifically and allows more flexibility in the cruise speed. Finally, in [11], a similar study is performed but focusing for departures. It aims at the quantification in terms of fuel and time consumption of implementing sub optimal trajectories in a 4D trajectory context that use RTAs at specific navigation fixes.

II. Concept of Operations

This section describes the concept of operations proposed in this work. Two strategies are considered: one where aircraft are allowed to fly powered descents and fly the initially planned route and another one where the route is stretched and the aircraft fly neutral CDOs.

Figure 1(a) depicts the vertical perspective of the first scenario used to illustrate the problem addressed in this work. Suppose an aircraft trying to land at a given airport with only one available arrival route. Well before the top of descent (TOD), while still in cruise, the aircraft is requested to compute its arrival time window at the metering fix, which is the difference between the earliest and the latest time of arrival at that fix (RTA_E and RTA_L), which are assumed to be computed by the FMS of the incoming aircraft by considering the earliest and latest trajectories.

One interesting matter is the width of this time window, which depends on several factors, e.g. the aircraft performance, weather conditions, etc. However, there is another factor that could be changed in order to obtain wider or shorter time windows, which is the type of descent being considered. Neutral CDOs assume idle thrust and no speed-brakes usage throughout the descent, while non-neutral or powered descents allow the use of thrust and speed-brakes. This supposes a higher flexibility with respect to neutral CDOs, which leads to wider time windows, but at the expense of increasing the fuel burnt and/or noise nuisance.

In addition to the neutral and powered time windows ($[RTA_{E_n}, RTA_{L_n}]$ and $[RTA_{E_p}, RTA_{L_p}]$ in Figure 1(a) respectively), aircraft send to the ATCO their estimated time of arrival. It should be noted that, while the earliest and latest times of arrival at the metering fix will mainly depend on aircraft performance, flight envelope and weather conditions; the estimated time of arrival at the same fix will be obtained after computing the optimal descent trajectory for that particular flight, subject to airline and crew policies, such for example, the Cost Index setting for that particular flight[1].

With all this information, ATC can assign an RTA at the metering fix to the arriving aircraft while it is still in cruise. In this way, the FMS on-board can compute the optimum CDO that complies with the RTA.

The vertical and lateral profiles of the second scenario are depicted in a simplified way in Figures 1(b) and 2, respectively. In this case, it is assumed that ATC could issue path stretching instructions, so in the end there is more than one arrival route available for the arriving aircraft. In order to illustrate this, a finite set of available arrival routes ($R_{a_0}, ..., R_{a_n}$ in Figure 2) with associated distances to go ($D_{a_0}, ..., D_{a_n}$ in Figure 1(b)) are defined. The process is the same as in the first scenario: aircraft send to the ATC their time window and ETA at the metering fix, and the ATC assigns them an RTA. However, in this case only neutral CDOs are allowed. In this paper the arrival route is considered to be pre-negotiated before the top of descent (TOD), as discussed in [13], so the FMS could know the remaining distance to go when the RTA is assigned at the metering fix.

[1]The Cost Index is a parameter chosen by the airspace user that reflects the relative importance of the cost of time with respect to fuel costs [12]

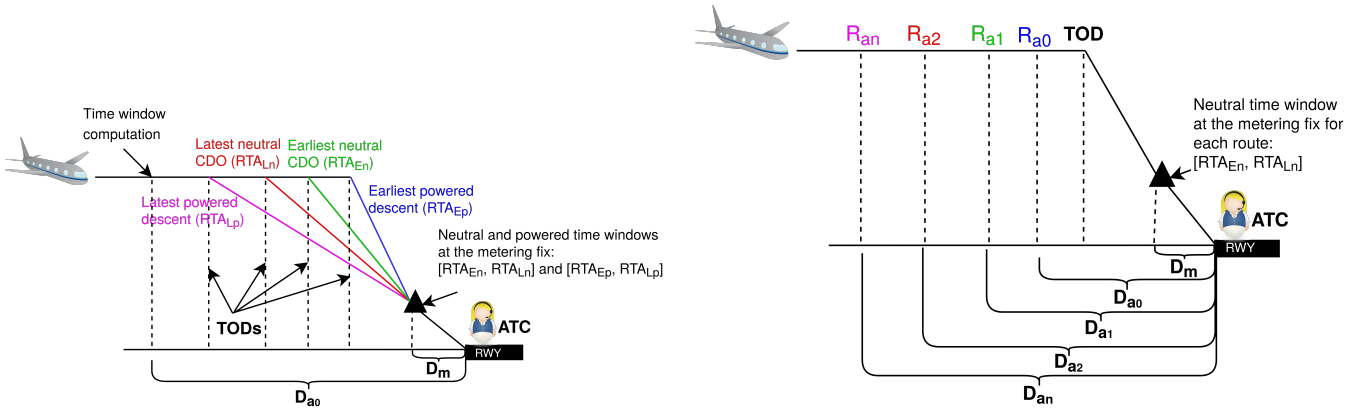

(a) Neutral CDO/powered descent

(b) Path stretching

Fig. 1: Vertical profile of both scenarios

Finally, in both scenarios the distance from the metering fix (where the RTA is assigned) to the runway remains the same.

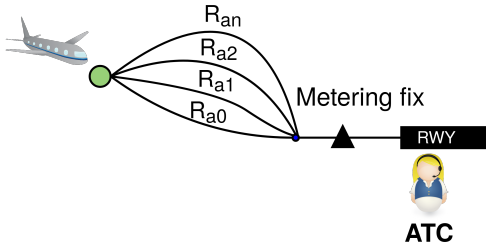

Fig. 2: Scenario 2: path stretching lateral profile

III. Trajectory optimization

This section presents the methodology used to generate the (optimal) trajectories for the validation scenario of this paper. In real life, these trajectories would be generated by an advanced functionality of each aircraft flight management system (FMS), assuming it is equipped with the RTA functionality.

In this paper, several trajectories are generated for the aircraft arriving at the airport subject of study; they are computed for different required times of arrival within the available metering fix time window and for several route lengths (i.e. distances to go).

Given a known lateral route, and consequently a fixed distance to go, the optimization of the vertical profile (altitude and speed) can be formulated as an optimal control problem, which aims at computing the control time history of a system, here the aircraft, such that a cost function is minimized while satisfying some dynamic and operational constraints. Several approaches can be found in the literature addressing this problem, like the ones found in [14] and [15], which focused on the development of advanced concepts and technologies in order to satisfy RTAs with high accuracy. In this work, the solution chosen is a non linear programming (NLP) trajectory optimizer like the one used in [16], which proved to be very robust and fast. The interior point optimizer (IPOPT) software package is used to solve the NLP problem.

Section III-A presents the optimal control problem in the continuous domain. Then, Section III-B shows how this problem is discretized. Finally, Section III-C details the optimal control problem particularized for aircraft descents.

A. Optimal control problem in the continuous domain

An optimal control problem over a fixed or variable continuous time horizon $[t_I, t_F]$ can be formulated as [17]:

$$\begin{aligned} \min_{\boldsymbol{u}(t)} \quad & J := \phi\left(\boldsymbol{x}(t_F), \boldsymbol{d}\right) + \int_{t_I}^{t_F} \pi\left(\boldsymbol{x}(t), \boldsymbol{u}(t), \boldsymbol{d}\right) \mathrm{d}t \\ \text{s.t} \quad & \boldsymbol{x}(t_I) = \boldsymbol{X} \\ & \dot{\boldsymbol{x}} = \boldsymbol{f}\left(\boldsymbol{x}(t), \boldsymbol{u}(t), \boldsymbol{d}\right) \\ & \boldsymbol{b}^{in}\left(\boldsymbol{x}(t), \boldsymbol{u}(t), \boldsymbol{d}\right) \leq 0 \\ & \boldsymbol{b}^{eq}\left(\boldsymbol{x}(t), \boldsymbol{u}(t), \boldsymbol{d}\right) = 0 \\ & \boldsymbol{\psi}\left(\boldsymbol{x}(t_F), \boldsymbol{d}\right) = 0, \end{aligned} \tag{1}$$

where $\boldsymbol{x} \in \Re^{n_x}$ is the vector of differential states; $\boldsymbol{u} \in \Re^{n_u}$ is the vector of controls; and $\boldsymbol{d} \in \Re^{n_d}$ is the vector of fixed parameters of the model. The cost function $J : \Re^{n_x} \times \Re^{n_u} \times \Re^{n_d} \rightarrow \Re$, which is composed by a running cost (or Lagrange term) $\pi : \Re^{n_x} \times \Re^{n_u} \times \Re^{n_d} \rightarrow \Re$ and an end cost (or Mayer term) $\phi : \Re^{n_x} \times \Re^{n_d} \rightarrow \Re$, is to be minimized subject to: dynamic constraints $\boldsymbol{f} : \Re^{n_x} \times \Re^{n_u} \times \Re^{n_d} \rightarrow \Re^{n_x}$ in the form of ordinary differential equations (ODEs) with initial conditions $\boldsymbol{X} \in \Re^{n_x}$; algebraic constraints $\boldsymbol{b}^{eq} : \Re^{n_x} \times \Re^{n_u} \times \Re^{n_d} \rightarrow \Re^{n_\varphi}$; inequality path constraints $\boldsymbol{b}^{in} : \Re^{n_x} \times \Re^{n_u} \times \Re^{n_d} \rightarrow \Re^{n_b}$; and terminal constraints $\boldsymbol{\psi} : \Re^{n_x} \times \Re^{n_d} \rightarrow \Re^{n_\psi}$.

Essentially, two different methods are available for solving Eq. (1): indirect methods, which involve the calculus of variations or the maximum principle of Pontryagin [17]; and direct methods, which transform the original infinite-dimensional optimal control problem into a finite-dimensional non-linear programming (NLP) optimization problem [18].

In this work, direct methods are used. These methods discretize the time histories of the control and/or state variables at a set of time samples. The cost function and constraints of the optimal control problem can be expressed in terms of these discretized states and/or controls, which become the decision variables of a parametric NLP optimization problem that can be solved by means of standard solvers.

B. Optimal control problem discretization using direct methods

Let the continuous time horizon $[t_I, t_F]$ be discretized into $N+1$ equidistant time samples τ_k, with $k = 0, \ldots, N$. Note that $\tau_0 = t_I$, $\tau_N = t_F$ and the discretization step is $\Delta\tau = {}^{(\tau_N - \tau_0)}/_{N}$. The discrete optimal control problem minimizing the cost function J in a time horizon of N time intervals can be formulated as:

$$\begin{aligned} \min_{\substack{\boldsymbol{x}_k, k=0,\ldots,N \\ \boldsymbol{u}_k, k=0,\ldots,N-1}} \quad & J := \phi\left(\boldsymbol{x}_N, \boldsymbol{d}\right) + \sum_{k=0}^{N-1} \Pi\left(\boldsymbol{x}_k, \boldsymbol{u}_k, \boldsymbol{d}, \Delta\tau\right) \\ \text{s.t} \quad & \boldsymbol{x}_0 = \boldsymbol{X} \\ & \boldsymbol{x}_{k+1} = \boldsymbol{F}\left(\boldsymbol{x}_k, \boldsymbol{u}_k, \boldsymbol{d}, \Delta\tau\right); \;\; k = 0, \ldots, N-1 \\ & \boldsymbol{b}^{in}\left(\boldsymbol{x}_k, \boldsymbol{u}_k, \boldsymbol{d}\right) \leq 0; \;\; k = 0, \ldots, N-1 \\ & \boldsymbol{b}^{eq}\left(\boldsymbol{x}_k, \boldsymbol{u}_k, \boldsymbol{d}\right) = 0; \;\; k = 0, \ldots, N-1 \\ & \boldsymbol{\psi}\left(\boldsymbol{x}_N, \boldsymbol{d}\right) = 0, \end{aligned} \tag{2}$$

where $\boldsymbol{x}_k \in \Re^{n_x}$ and $\boldsymbol{u}_k \in \Re^{n_u}$ are the state and control vectors discretized at τ_k, respectively, for $k = 0, \ldots, N$.

The optimal control problem described by Eq. (2) assumes that the same running cost, dynamic constraints and algebraic and path constraints apply during the whole time horizon. In addition, event constraints can be set only at the very end of the time horizon. Yet, many *real-life* processes can be divided into several phases (or stages), where the dynamics of the system, the running cost and the algebraic and path constraints might change. In addition, in some particular applications it

is necessary to formulate interior-point constraints in between two consecutive phases.

Eq. (2) can be easily extended to multi-phase problems. First, let the continuous time horizon $[t_I, t_F]$ be divided into P time intervals $[t_j, t_{j+1}]$ for $j = 0, \ldots, P-1$; each time interval corresponding to a different phase. Again, $t_0 = t_I$ and $t_P = t_F$. Then, each time intervals (or phase) is discretized into N_j equidistant time samples $\tau_k, \tau_{k+1}, \ldots, \tau_{k+N_j-1}$, where $\tau_k = t_j$, $\tau_{k+N_j-1} = t_{j+1}$ and $k = \sum_{i<j} N_i$, for all $j = 0, \ldots, P-1$. The discretization step of the j^{th} phase is denoted by $\Delta\tau_j$. As a result, the whole time horizon is discretized into $N+1 = \sum_{j=0}^{P-1} N_j$ time samples $\tau_0, \tau_1, \ldots, \tau_N$.

Let $\mathcal{T}$ be a multi-dimensional set that relates the index of each phase to the indexes of its corresponding time samples. The subset $\mathcal{E} \subseteq \mathcal{T}$ only includes the index corresponding to the last time sample of each phase; and $\mathcal{I}$ is defined as $\mathcal{T} \backslash \mathcal{E}$.

Based on the definitions stated above, the discrete multi-phase optimal control problem can be formulated as:

$$
\begin{aligned}
\min_{\substack{\boldsymbol{x}_k, k=0,\ldots,N \\ \boldsymbol{u}_k, \forall (j,k) \in \mathcal{I}}} \quad & J := J_a + J_b \\
& J_a = \sum_{(j,k)\in\mathcal{E}} \phi_j \left(\boldsymbol{x}_k, \boldsymbol{d}\right) \\
& J_b = \sum_{(j,k)\in\mathcal{I}} \Pi_j \left(\boldsymbol{x}_k, \boldsymbol{u}_k, \boldsymbol{d}, \Delta\tau_j\right) \\
\text{s.t} \quad & \boldsymbol{x}_0 = \boldsymbol{X} \\
& \boldsymbol{x}_{k+1} = \boldsymbol{F}_j \left(\boldsymbol{x}_k, \boldsymbol{u}_k, \boldsymbol{d}, \Delta\tau_j\right); \forall (j,k) \in \mathcal{I} \\
& \boldsymbol{b}_j^{in} \left(\boldsymbol{x}_k, \boldsymbol{u}_k, \boldsymbol{d}\right) \leq 0; \forall (j,k) \in \mathcal{I} \\
& \boldsymbol{b}_j^{eq} \left(\boldsymbol{x}_k, \boldsymbol{u}_k, \boldsymbol{d}\right) = 0; \forall (j,k) \in \mathcal{I} \\
& \boldsymbol{\vartheta}_j^{eq} \left(\boldsymbol{x}_k, \boldsymbol{d}\right) = 0; \forall (j,k) \in \mathcal{E} \backslash \{(P-1, N)\} \\
& \boldsymbol{\vartheta}_j^{in} \left(\boldsymbol{x}_k, \boldsymbol{d}\right) \leq 0; \forall (j,k) \in \mathcal{E} \backslash \{(P-1, N)\} \\
& \boldsymbol{\psi} \left(\boldsymbol{x}_N, \boldsymbol{d}\right) = 0 \\
& \boldsymbol{x}_k - \boldsymbol{x}_{k+1} = 0; \forall (j,k) \in \mathcal{E} \backslash \{(P-1, N)\}
\end{aligned}
\tag{3}
$$

In Eq. (3), $\Pi_j : \Re^{n_x} \times \Re^{n_u} \times \Re^{n_d} \times \Re \to \Re$ and $\boldsymbol{F}_j : \Re^{n_x} \times \Re^{n_u} \times \Re^{n_d} \times \Re \to \Re^{n_x}$ are the quadrature and states evolution functions for the j^{th} phase, respectively. Similarly, $\boldsymbol{b}_j^{eq} : \Re^{n_x} \times \Re^{n_u} \times \Re^{n_d} \to \Re^{n_{\varphi_j}}$ and $\boldsymbol{b}_j^{in} : \Re^{n_x} \times \Re^{n_u} \times \Re^{n_d} \to \Re^{n_{b_j}}$ are the algebraic and path constraints, respectively, of the j^{th} phase; and $\boldsymbol{\vartheta}_j^{eq} : \Re^{n_x} \times \Re^{n_d} \to \Re^{n_{\vartheta_j^{eq}}}$, and $\boldsymbol{\vartheta}_j^{in} : \Re^{n_x} \times \Re^{n_d} \to \Re^{n_{\vartheta_j^{in}}}$ represent applicable equality and inequality interior-point constraints, respectively, applying at the last time of the j^{th} phase. Note that in Eq. (3) a new set of constraints has been added to link the state variables across two consecutive phases and guarantee continuity in the solution.

Analogously to the single-phase optimal control problem, the discretization step of each individual phase could be considered either a known parameter or variable to be optimized, depending on the context. For instance, if the duration of the whole time horizon were fixed to a certain parameter, say a RTA, but the duration of each phase were flexible, $\Delta\tau_j$ for $j = 0, \ldots, P-1$ would become decision variables subject to the following constraint:

$$
\sum_{j=0}^{P-1} \left(N_j - 1\right) \Delta\tau_j - \text{RTA} = 0, \tag{4}
$$

which would be appended to Eq. (3).

C. Optimal control problem for aircraft descents

For the remainder of this document the optimal control problem will be formulated in the continuous domain aiming to keep the notation simple. However, the problem needs to be discretized.

The state vector $\boldsymbol{x} = [t, v, h]$ is composed of time, true airspeed (TAS), and altitude; the control vector $\boldsymbol{u} = [\gamma, T, \beta]$ is composed of the aerodynamic flight path angle, engine thrust, and speed brakes deflection. The flight path angle is the control that is used by the aircraft to modulate energy (i.e., exchange potential energy for kinetic energy and vice-versa), whereas thrust and speed brakes are used to add and remove energy from the system, respectively.

Different from typical formulations, the independent variable in this problem is the distance to go (s) and not the time [16]. The selection of s as the independent variable is driven by the fact that during an ideal CDO, with no intervention from the air traffic controllers (ATC) except for the assignment of the RTA, the aircraft will follow a "closed route", and therefore the remaining distance to go will be always known by the FMS. In addition, this formulation replicates how constraints are defined in the current operational environment, thereby enabling more precise modeling of the constraints.

The dynamics of $\boldsymbol{x}$ are expressed by the following set of ordinary differential equations, considering a point-mass representation of the aircraft reduced to a 'gamma-command" model, where vertical equilibrium is assumed (lift balances weight) and the cross and vertical components of the wind are neglected:

$$
\boldsymbol{f}_j = \frac{\mathrm{d}\boldsymbol{x}}{\mathrm{d}s} = \begin{bmatrix} 1 \\ \frac{T - D(v,h,\beta)}{m} - g\sin\gamma \\ v\sin\gamma \end{bmatrix} \frac{1}{v\cos\gamma + w(h)} \tag{5}
$$

where $D : \mathbb{R}^{n_x \times n_u} \to \mathbb{R}$ is the aerodynamic drag; g is the gravity acceleration and m the mass, which is assumed to be constant since the fuel consumption during a descent is a small fraction of the total mass [3]. In this paper it has been assumed that the effect of the cross-wind on the ground speed is orders of magnitude below that of the longitudinal wind, like done in previous works [19].

The longitudinal component of the wind $w : \mathbb{R} \to \mathbb{R}$ is modeled by a smoothing spline as function of the altitude:

$$
w(h) = \sum_{i=1}^{n_c} c_i B_i(h), \tag{6}
$$

where B_i, $i = 1, \ldots, n_c$, are B-spline basis functions and $\boldsymbol{c} = [c_1, \ldots, c_{n_c}]$ are control points of the spline [20]. It should

be noted that the longitudinal wind has been modeled as a function of the altitude only, as done in other research [21].

Since the flight time is fixed by the RTA, the goal is to minimize a fuel consumption for the remaining descent. Therefore, the stage cost is:

$$\pi_j(v,h,T,\gamma) = \frac{q(v,h,T)}{(v\cos\gamma + w(h))} \tag{7}$$

where $q : \mathbb{R}^{n_x \times n_u} \to \mathbb{R}$ is the fuel flow and K_β a weighting parameter that determines how much the use of β is penalized. It should be noted that in this application example, no terminal cost are considered (i.e., $\phi_j = 0$ for $j = 0, \ldots, P-1$). Furthermore, a fourth-order Runge-Kutta scheme is used to obtain $\boldsymbol{F}_j$ and Π_j from $\boldsymbol{f}_j$ and π_j, respectively.

In addition, the following terminal constraints are enforced at the end of the trajectory:

$$\boldsymbol{\psi} = \begin{bmatrix} v_{CAS}(v,h) - v_{CAS_F} \\ h - h_F \end{bmatrix}, \tag{8}$$

where $v_{CAS} : \mathbb{R}^{n_x} \to \mathbb{R}$ is the calibrated airspeed (CAS); and v_{CAS_F} and h_F are the CAS and altitude at the runway, respectively.

Phase-independent path constraints on the controls (i.e., applying all along the descent) are also considered, aiming to ensure that the maximum and minimum descent gradients, thrust and speed brakes are not exceeded:

$$\boldsymbol{b}_j^{in} = \begin{bmatrix} \gamma \\ \gamma_{min} - \gamma \\ T_{min}(v,h) - T, T - T_{max}(v,h) \\ 0.0 - \beta \\ \beta - 1.0 \end{bmatrix} \tag{9}$$

where γ_{min} is the minimum descent gradient; $T_{min} : \mathbb{R}^{n_x} \to \mathbb{R}$ and $T_{max} : \mathbb{R}^{n_x} \to \mathbb{R}$ are the idle and maximum thrust, respectively; $\beta = 0$ and $\beta = 1$ indicate that speed brakes are retracted and fully extended, respectively. Different alternatives can be used to model T_{min}, T_{max}, D and q and their respective parameters. In this paper, the EUROCONTROL's base of aircraft data (BADA) v4 model has been adopted [22]. However, BADA v4 does not include a model for the effects of the speed brakes on the drag coefficient C_D. As a workaround, in this paper the contribution of the speed brakes has been modeled as an extra linear term $C_{D_\beta}\beta$ in the generic BADA v4 drag coefficient model, where C_{D_β} is a coefficient representing the increase in drag coefficient for unit of speed brakes deflection. More specifically, the speed brakes deflection can take the following values: [0.0, 0.5, 1.0] (i.e. [null, half, full]).

The descent can be divided into several phases, defined between two consecutive waypoints of the trajectory with associated speed and/or altitude constraints. In each phase, different operational constraints may apply and may be modeled in the form of additional path, algebraic and interior-point constraints, which depend on the particular procedure being investigated and that will be listed in Section IV-A. Finally, it is assumed that during the cruise phase the speed remains constant.

IV. Results

This section presents the results obtained in this work. Section IV-A describes the experimental setup used to illustrate the methodology proposed in this paper. Then, Section IV-B shows the trajectories obtained with the trajectory optimizer for the neutral CDOs and powered descents. Finally, Section IV-C shows the fuel consumption results, comparing the two strategies described in Section II: descent type and path stretching.

A. Experimental setup

An Airbus A320-231 is chosen for the experiment, assuming a cruise altitude of FL360 and a Mach of 0.78. Well before starting the descent, the optimal descent trajectory to the runway for a typical cost index of $30\,\text{kg min}^{-1}$ [12] is computed, discretizing the continuous optimal control problem into $N = 115$ time samples. A higher number of time samples (shorter interval duration) results in a more accurate solution, however, the computational burden becomes greater. As a result of this optimization, the optimal time of arrival at the metering fix is obtained, which corresponds to the ETA at that fix. International standard atmosphere (ISA) conditions and no wind are considered when generating the trajectories.

As explained in Section II, two scenarios are considered in this paper. The distance to go considered in the neutral CDO/powered descent scenario is 180 NM, while for the path stretching scenario the distances considered range from 150 NM to 250 NM in 10 NM steps (i.e. 11 possible routes or distances to go). The metering fix, where the RTA is fixed, is set at an altitude of 3,000 ft, at a distance of 18 NM from the runway.

Several RTAs are defined at the metering fix. They are computed as a function of the ETA and the time window. In total, 20 RTAs are defined: 10 earlier and 10 later than the ETA. They are equally spaced in time within the available powered time window. The same RTAs are considered for both scenarios; in this way, it is possible to compute and compare the fuel consumption in both cases depending on how far the RTA is defined with respect to the ETA.

Constraints are required to model the vertical profile. In order to accomplish that, the descent is divided in $P = 2$ different phases from the start of the descent until the metering fix, with associated phase-dependent path, along with algebraic and/or interior-point constraints. Table I wraps up these phases and their associated constraints.

where $M : \mathbb{R}^{n_x} \to \mathbb{R}$ is the Mach number; MMO and VMO are the maximum operative Mach and CAS, respectively; and GD is the green dot speed[2].

For the path constraints of the generic model (see Eq. (9)), the minimum descent gradient is set to $-7°$. In addition, the

[2]For the Airbus A320, the green dot speed is the minimum operating speed in managed mode and clean configuration, being approximately the best lift-to-drag ratio speed

TABLE I: Phases and associated constraints until the metering fix for a generic arrival procedure

Phase	$\boldsymbol{b}_j^{in}$	$\boldsymbol{\varphi}_j^{eq}$	$\boldsymbol{\vartheta}_j^{in}$	$\boldsymbol{\vartheta}_j^{eq}$
1	$\begin{bmatrix} M - \text{MMO} \\ v_{CAS} - \text{VMO} \\ GD - v_{CAS} \end{bmatrix}$	-	$\begin{bmatrix} 250\,\text{kt} - v_{CAS} \\ v_{CAS} - GD \end{bmatrix}$	$\begin{bmatrix} h - 10,000\,\text{ft} \end{bmatrix}$
2	$\begin{bmatrix} v_{CAS} - 210\,\text{kt} \\ 190\,\text{kt} - v_{CAS} \end{bmatrix}$	-	-	$\begin{bmatrix} h - 3,000\,\text{ft} \end{bmatrix}$

values for VMO and MMO are obtained from the BADA v4 global parameters file. Furthermore, additional thrust and the use of speed-brakes (T and β respectively) are only allowed for powered descents.

It should be noted that nominal flap/slat (and landing gear) transitions are also considered as additional trajectory phases (there are a total of 7 more phases), but are not depicted in Table I. Finally, the terminal constraints of the generic model (see Eq. (8)) are set at the runway, such that $h_F = 50\,\text{ft}$ and $v_{CAS_F} = 138\,\text{kt}$.

B. Earliest and latest trajectories

For illustrative purposes, Figure 3 shows the evolution of altitude and speed as a function of the remaining distance to the runway. The speed-brakes deflection is also shown. For all cases, the distance to go is 180 NM and the cruise speed is kept constant until the top of descent.

In the earliest neutral case (Figure 3(a)) it is observed how the aircraft accelerates to MMO right after the TOD. This descent at constant Mach implies an increase of the CAS and, when reaching the VMO, the descent continues at this maximum speed down to FL100, where a deceleration is performed to comply with the 250 kt speed limit on CAS. Figure 3(b), in turn, shows the latest neutral trajectory, which slows down to the minimum allowed speed (GD) right after the TOD. This speed is maintained until few nautical miles before arriving to the runway, where another deceleration is performed. In both neutral cases, no speed-brakes are used, as the aircraft is performing a neutral CDO.

As expected, the results for the powered trajectories are different, as the energy of the aircraft can be increased or decreased by means of additional thrust and speed-brakes use. In both earliest/latest cases, the descent starts before than in the neutral cases. The earliest powered trajectory (Figure 3(c)) uses the elevator to descend the fastest possible and accelerate to MMO. This descent is maintained until both VMO and MMO are achieved, at an altitude close to the crossover altitude, where the TAS is maximized. Then, the

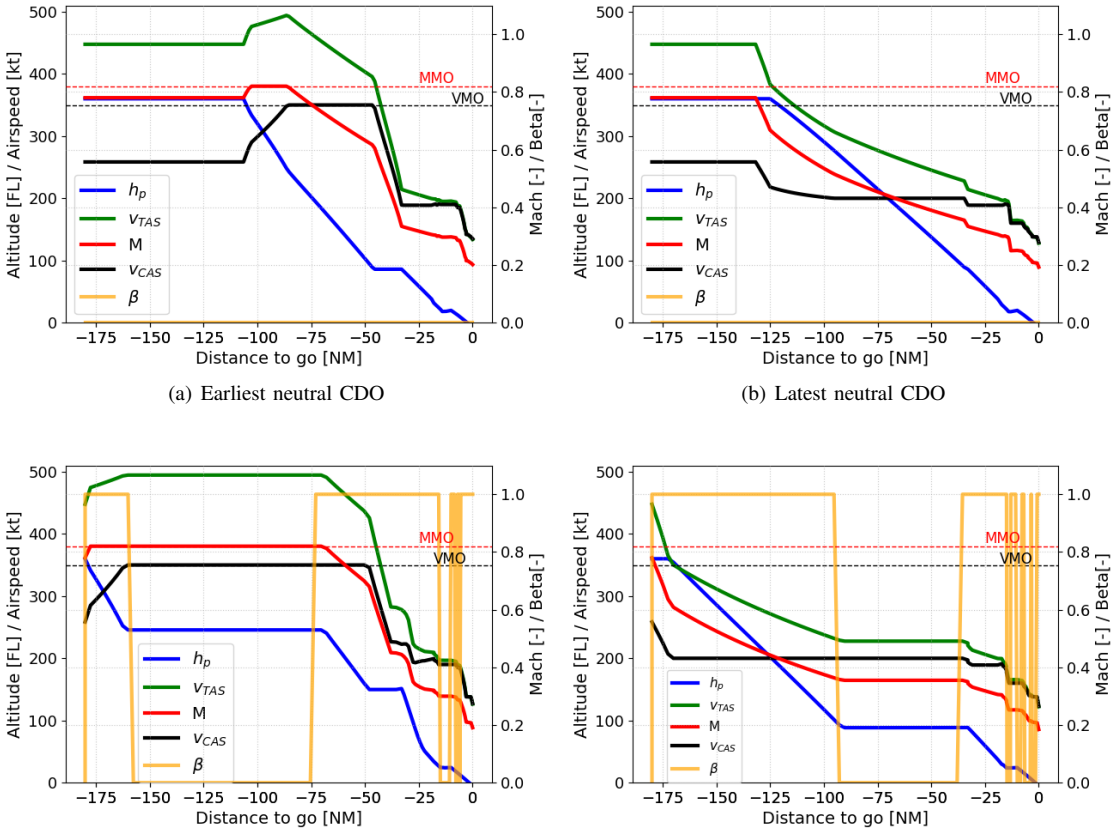

(a) Earliest neutral CDO

(b) Latest neutral CDO

(c) Earliest powered descent

(d) Latest powered descent

Fig. 3: Earliest and latest trajectories (Airbus A320-231)

altitude and speed are kept constant until a deceleration is performed to comply with the FL100 speed limit. In the latest powered case (Figure 3(d)), a descent at the maximum descent gradient is performed in order to release potential energy as fast as possible. In addition, speed-brakes are deployed during this phase in order to decrease the speed of the aircraft until GD speed is reached. In both powered cases speed-brakes are used intermittently in the latter stages of the trajectory to control the aircraft and keep an adequate speed for landing.

C. Fuel consumption comparison between descent type vs. path stretching strategies

Figure 4 shows the fuel consumption for the two strategies compared in this paper when an RTA different from the aircraft's ETA is assigned. The x-axis represents the RTA time difference with respect to the ETA (located at 0) and the y-axis represents the fuel consumption in kg. It has to be taken into account that the cost index used to compute the ETA is 30 kg/min, so the lowest fuel consumption does not correspond to the trajectory arriving at the metering fix at that time. As a result, for times immediately after the ETA the fuel consumption decreases for both strategies.

Figure 4 leads to several interesting conclusions. First of all, it is observed that for RTAs lying in the neutral time window (the shaded area in the graph) both strategies show the same behavior in terms of fuel consumption. This is understandable as in both cases the aircraft performs a neutral CDO and the route length remains the same. However, different results can be observed when the RTA lies outside the neutral time window. For RTAs later than the ETA, and if the path is not stretched, aircraft are forced to fly powered descents in order to meet the time constraint, which supposes an increase in fuel consumption. This is observed in the blue line. On the other hand, for a same RTA outside the neutral time window and if aircraft fly neutral CDOs, the path needs to be stretched in order to meet that time constraint. As a result, the fuel consumption increases too, as it is observed in the orange line. However, the increase in fuel consumption is not the same in both strategies. At the beginning, the path stretching strategy, where aircraft fly for a longer time in cruise and a for a longer route distance, supposes a higher fuel consumption. However, as the RTA assigned is further from the ETA, the fuel consumed when flying powered descents increases drastically, ending up with a higher consumption value than the path stretching strategy, even when the distance flown is lower. Finally, for RTAs outside the neutral time window and before the ETA, flying powered descents leads to a higher fuel consumption than in the path stretching case. In this situation, and to meet a same RTA, the route is shortened if neutral CDOs are flown. If the route distance remains constant, a powered descent is flown.

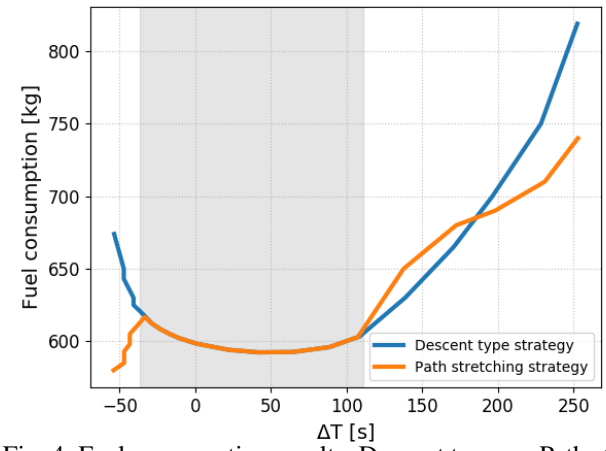

Fig. 4: Fuel consumption results: Descent type vs. Path stretching

V. Conclusions

This paper quantified the fuel consumption when aircraft are assigned an RTA different from their ETA. Two strategies were compared, one in which aircraft fly the planed route but are forced to fly powered descents and another one where the route is stretched and neutral CDOs are flown. Results show that, for RTAs later than the ETA, although in the beginning path stretching represents a higher fuel consumption, in the end flying powered descents is the strategy that consumes more fuel. On the other hand, for RTAs earlier than the ETA, path stretching represents an advantage with respect to powered descents in terms of fuel consumption as shorter routes are flown.

The results obtained in this work could be a starting point towards defining a ground supporting tool to help ATC to decide which would be the best decision under the TBO paradigm, where advanced synchronisation mechanisms between ground and airborne tools are expected. This work could also mean an improvement on some of the authors' previous works like [13], focusing on sequencing and merging traffic in TMA. When it is not possible to schedule all aircraft by flying neutral CDOs, maybe flying powered descents or stretching the route could help to accommodate all traffic and keep the safety of the operation.

In the work presented in this paper, only one aircraft model was considered, and the same initial conditions were assumed for all cases. This is not a representative enough scenario to conclude the behavior in terms of fuel consumption of flying powered descents vs. flying longer routes. Other factors like the wind or the aircraft mass could greatly affect the results too. Furthermore, in this study it is assumed that the RTA initially assigned to the aircraft would not vary during the whole trajectory. However, in some cases, the ATC could decide to issue a new RTA, so it is also important to take that into account when optimizing the trajectory and be able to adapt to RTA updates. In future work, a study in greater depth will be performed, aiming at providing a solution for a greater variety of scenarios.

REFERENCES

[1] L. Erkelens, "Research into new noise abatement procedures for the 21st century," in *AIAA Guidance, Navigation, and Control Conference and Exhibit*, ser. Guidance, Navigation, and Control and Co-located Conferences. Denver, CO: American Institute of Aeronautics and Astronautics, 2000.

[2] A. Warren and K. Tong, "Development of continuous descent approach concepts for noise abatement," in *IEEE/AIAA 21st Digital Avionics Systems Conference (DASC)*, Irvine, CA, 2002.

[3] J. P. B. Clarke, N. T. Ho, L. Ren, J. A. Brown, K. R. Elmer, K. F. Zou, C. Hunting, D. L. McGregor, B. N. Shivashankara, K. Tong, A. W. Warren, and J. K. Wat, "Continuous descent approach: Design and flight test for Louisville international airport," *Journal of Aircraft*, vol. 41, no. 5, pp. 1054–1066, 2004.

[4] SESAR Joint Undertaking, "European ATM Master Plan. The roadmap for delivering high performing aviation for Europe," Brussels, Tech. Rep., 2015.

[5] Federal Aviation Administration (FAA), "Nextgen implementation plan 2016," Tech. Rep., 2016.

[6] J. K. Klooster, A. D. Amo, and P. Manzi, "Controlled Time-of-Arrival Flight Trials," in *8th USA/Europe air traffic management research and development seminar*, Napa, CA, 2009.

[7] R. Dalmau and X. Prats, "Controlled time of arrival windows for already initiated energy-neutral continuous descent operations," *Transportation Research Part C: Emerging Technologies*, vol. 85, pp. 334 – 347, 2017.

[8] A. Pawełek, P. Lichota, R. Dalmau, and X. Prats, "Fuel-efficient trajectories traffic synchronization," *Journal of aircraft*, vol. 56, no. 2, pp. 481 – 492, Mar 2019.

[9] R. Dalmau, J. Alenka, and X. Prats, "Combining the assignment of pre-defined routes and RTAs to sequence and merge arrival traffic," in *17th AIAA Aviation Technology, Integration, and Operations Conference (ATIO)*, Denver, CO, 2017.

[10] T. Nikoleris, G. B. Chatterji, and R. A. Coppenbarger, "Comparison of fuel consumption of descent trajectories under arrival metering," *Journal of Aircraft*, vol. 53, no. 6, Nov 2016.

[11] S. Vilardaga and X. Prats, "Operating cost sensitivity to required time of arrival commands to ensure separation in optimal aircraft 4d trajectories," *Transportation Research Part C: Emerging Technologies*, vol. 61, pp. 75–86, Dec 2015.

[12] Airbus, "Getting to grips with the cost index," Flight Operations Support and Line Assistance, Blagnac, France, Tech. Rep., 1998.

[13] R. Sáez, R. Dalmau, and X. Prats, "Optimal assignment of 4D close-loop instructions to enable CDOs in dense TMAs," in *Proceedings of the 37th IEEE/AIAA Digital Avionics Systems Conference (DASC)*. IEEE and AIAA, Sep 2018.

[14] P. M. A. de Jong, F. J. L. Bussink, R. Verhoeven, N. de Gelder, M. M. V. Paassen, and M. Mulder, "Time and Energy Management during Descent and Approach: a human-in-the-loop study," *Journal of Aircraft*, vol. 54, no. 1, pp. 177–189, 2017.

[15] X. Prats, R. Dalmau, R. Verhoeven, and F. Bussink, "Human-in-the-loop performance assessment of optimized descents with time constraints. results from full motion flight simulation and a flight testing campaign," in *Proceedings of the 12th USA/Europe Air Traffic Management Research and Development Seminar*. Seattle, WA (USA): Eurocontrol and FAA, Jun 2017.

[16] R. Dalmau, X. Prats, and B. Baxley, "Using wind observations from nearby aircraft to update the optimal descent trajectory in real-time," in *Proceedings of the 13th USA/Europe Air Traffic Management Research and Development Seminar*. Vienna (Austria): Eurocontrol and FAA, Jun 2019.

[17] A. E. Bryson and Y.-C. Ho, *Applied optimal control : optimization, estimation, and control*. New York, USA: Taylor and Francis Group, 1975.

[18] J. T. Betts, *Practical Methods for Optimal Control and Estimation Using Nonlinear Programming*, 2nd ed. SIAM, 2010.

[19] R. Dalmau, "Optimal trajectory management for aircraft descent operations subject to time constraints," PhD Thesis, Technical University of Catalonia (UPC), 2019.

[20] C. de Boor, "On calculating with B-splines," *Journal of Approximation Theory*, vol. 6, no. 1, pp. 50–62, 1972.

[21] P. M. A. de Jong, J. J. van der Laan, A. C. Veld, M. M. van Paassen, and M. Mulder, "Wind-Profile Estimation Using Airborne Sensors," *Journal of Aircraft*, vol. 51, no. 6, pp. 1852–1863, 2014.

[22] D. Poles, A. Nuic, and V. Mouillet, "Advanced aircraft performance modelling for ATM: Analysis of BADA model capabilities," in *29th Digital Avionics Systems Conference*. Brétigny-sur-Orge (France): EUROCONTROL, 2010.